The influence of the waveguide layer composition on the emission parameters of 1550 nm InGaAs/InP laser heterostructures

© I.I. Novikov[1], I.A. Nyapshaev[1], A.G. Gladyshev[1], V.V. Andryushkin[1], A.V. Babichev[1], L.Yu. Karachinsky[1], Yu.M. Shernyakov[2], D.V. Denisov[3,4], N.V. Kryzhanovskaya[5], A.E. Zhukov[5], A.Yu. Egorov[6]

[1] ITMO University,
197101 St. Petersburg, Russia
[2] Ioffe Institute,
194021 St. Petersburg, Russia
[3] Connector Optics LLC,
194292 St. Petersburg, Russia
[4] St. Petersburg State Electrotechnical University „LETI",
197376 St. Petersburg, Russia
[5] National Research University Higher School of Economics,
190008 St. Petersburg, Russia
[6] Alferov Federal State Budgetary Institution of Higher Education and Science
Saint Petersburg National Research Academic University of the Russian Academy of Sciences,
194021 St. Petersburg, Russia

E-mail: Novikov@switch.ioffe.ru

Received May 20, 2022
Revised July 12, 2022
Accepted August 10, 2022

The influence of InGaAlAs waveguide composition on the photoluminescence and electroluminescence of 1550 nm spectral range heterostructures based on thin strained $In_{0.74}Ga_{0.26}As$ quantum wells has been studied. An approach is proposed that allows based on the analysis of electroluminescence to carry out a comparative analysis of the deferential gain in fabricated laser diodes. It is shown that decrease of the molar fraction of aluminum in waveguide InGaAlAs layers matched in lattice constant with InP leads to falling of integrated photoluminescence intensity, however, laser diodes with $In_{0.53}Ga_{0.31}Al_{0.16}As$ waveguide layers demonstrate a higher differential gain compared to laser diodes with $In_{0.53}Ga_{0.27}Al_{0.20}As$ waveguide.

Keywords: quantum well, molecular-beam epitaxy, photoluminescence, electroluminescence.

DOI: 10.21883/SC.2022.09.54140.9892

1. Introduction

The current research in semiconductor laser physics is aimed primarily at enhancing the dynamic performance of lasers an raising the frequency of their current modulation and, consequently, the data transmission rate in optical communication lines [1,2]. Particular attention is paid to vertical-cavity surface-emitting lasers (VCSELs), which are characterized by ultracompact sizes, low operating currents, and high energy efficiency [3]. Although considerable progress has been achieved in the development of VCSELs of the 1300−1550 nm spectral range [4–7], the obtained results still lag behind those achieved for shorter-wave vertical-cavity surface-emitting lasers of the 850−940 nm range [8]. This is largely attributable to the limitations of the InGaAlAsP/InP material system (compared to InGaAlAs/GaAs) and the infeasibility of monolithic integration on an efficient distributed Bragg reflector (DBR) and an efficient active region for wavelengths > 1200 nm in a single laser heterostructure and in one epitaxial process. The use of InGaAsN quantum wells on GaAs [9] and the metamorphic growth of quantum dots on GaAs [10] provides a partial solution to these problems, but the efficiency and speed performance of the fabricated VCSELs are still insufficient [11].

It has been demonstrated earlier that the method of semiconductor wafer fusing allows one to fabricate efficient VCSELs with modulation frequencies > 11 GHz [12] and data transmission rates > 25 Gbit/s [6]. The primary advantage of this approach consists in the proven reliability of such VCSELs, which were found to comply with the requirements of Telcordia GR-468-CORE [13]. It must be admitted that wafer-fused VCSELs still lag behind the lasers of the 1300−1550 nm spectral range produced using an alternative approach based on a dielectric DBR [4,7], where a record-high modulation frequency of ∼ 22 GHz at 25°C was achieved by reducing the thermal laser resistance and shortening the effective VCSEL cavity length [4]. However, this approach appear to offer less potential in terms of reliability and mass production of VCSELs, since it imposes stricter requirements regarding the optical uniformity of layers and the roughness of interfaces of dielectric DBRs. The optimization and enhancement of parameters of VCSELs produced by heterostructure fusion are associated

Description of test heterostructures*

Layer designation	Layer material	Layer thickness, nm	Number of repetitions
Covering layer	$In_{0.53}Ga_{0.47}As$	5	
Bounding layer	$In_{0.52}Al_{0.48}As$	30	
Matrix	1-$In_{0.53}Ga_{0.27}Al_{0.20}As$ (1220 nm) 2-$In_{0.53}Ga_{0.31}Al_{0.16}As$ (1300 nm) 3-$In_{0.53}Ga_{0.34}Al_{0.13}As$ (1350 nm)	38	
Barrier	1-$In_{0.53}Ga_{0.27}Al_{0.20}As$ (1220 nm) 2-$In_{0.53}Ga_{0.31}Al_{0.16}As$ (1300 nm) 3-$In_{0.53}Ga_{0.34}Al_{0.13}As$ (1350 nm)	12	9
Quantum well	$In_{0.74}Ga_{0.26}As$	2.9	9
Matrix	1-$In_{0.53}Ga_{0.27}Al_{0.20}As$ (1220 nm) 2-$In_{0.53}Ga_{0.31}Al_{0.16}As$ (1300 nm) 3-$In_{0.53}Ga_{0.34}Al_{0.13}As$ (1350 nm)	50	
Bounding layer	$In_{0.52}Al_{0.48}As$	200	
Substrate	InP		

Note. * The calculated maxima of PL from matrix/barrier $In_{0.53}Ga_xAl_{0.47-x}As$ layers are given in brackets.

primarily with the optimization of the heterostructure of the active region grown on an InP substrate, which is later fused with semiconductor AlGaAs/GaAs-based DBRs. We have demonstrated earlier that thin highly strained InGaAs quantum wells with a molar fraction of InAs exceeding 70% provide an opportunity to produce efficient VCSELs of the 1520–1580 nm spectral range [6]. In addition, the use of thin quantum wells (QWs) leads to expulsion of excited electron levels, and the doping of barrier layers of quantum wells with carbon at a level of $10^{12}\,cm^{-2}$ results in suppression of nonradiative recombination [14] and allows one to reduce the temperature coefficient of variation of the lasing wavelength in lasers based on such QWs and raise the characteristic temperature of the threshold current [15]. In the present paper, we report the results of studies into the influence of the molar composition of a waveguide InAlGaAs layer in an active region based on thin InGaAs QWs on the threshold characteristics and gain parameters of stripe lasers. The obtained data should be instrumental in further potential optimization of VCSELs with similar active regions.

2. Experiment

At the first stage, a series of test heterostructures with different compositions of matrix and barrier $In_{0.53}Ga_xAl_{0.47-x}As$ layers for photoluminescence studies were fabricated by molecular beam epitaxy performed using a RIBER 49 setup. These heterostructures are characterized in the table; note that two heterostructures with matrix/barrier $In_{0.53}Ga_{0.34}Al_{0.13}As$ layers were grown.

Photoluminescence (PL) of the fabricated test heterostructures with different matrix/barrier layers (see the table) was examined. The PL spectra of heterostructures were measured using a PM2000 VerteX (Nanometrics) setup with an InGaAs photodetector. Photoluminescence was excited by a laser operating at a wavelength of 532 nm. Its radiation was focused to a spot $\sim 100\,\mu m$ in size on the heterostructure surface. All heterostructures exhibited bright PL with a peak in the 1530–1560 nm range. Measurements at a high optical pumping power (42 mW) were performed in the course of examination. The variation of the peak/integral PL intensities with the calculated band gap of the matrix material in heterostructures is presented in Fig. 1. It can be seen that the PL intensity decreases with decreasing band gap (E_g) of the matrix/barirer layers. This is probably attributable to the thermal ejection of carriers. Therefore, the PL signal variation may be an ill-fitting tool for estimation of the active region gain in this case, and experimental studies of lasers based on heterostructures with a similar active region are needed for this purpose.

The dependence of the integral PL intensity on the optical pumping power allows one to estimate the relative contributions of different recombination processes to emission with the use of the so-called ABC-model of recombination processes [16,17]. Optical pumping power density P is proportional to the carrier generation rate:

$$P \sim An + Bn^2 + Cn^3, \quad (1)$$

where n is the carrier density in equilibrium (when the densities of electrons and holes are equal), An is the Shockley–Read–Hall (SRH) nonradiative recombination rate, Bn^2 is the radiative recombination rate, and Cn^3 is the Auger recombination rate. At low optical pumping levels (i.e., low densities n), the SRH recombination mechanism is dominant, while Auger recombination dominates at high optical pumping levels, since the terms with n raised to higher powers then naturally start producing a more significant

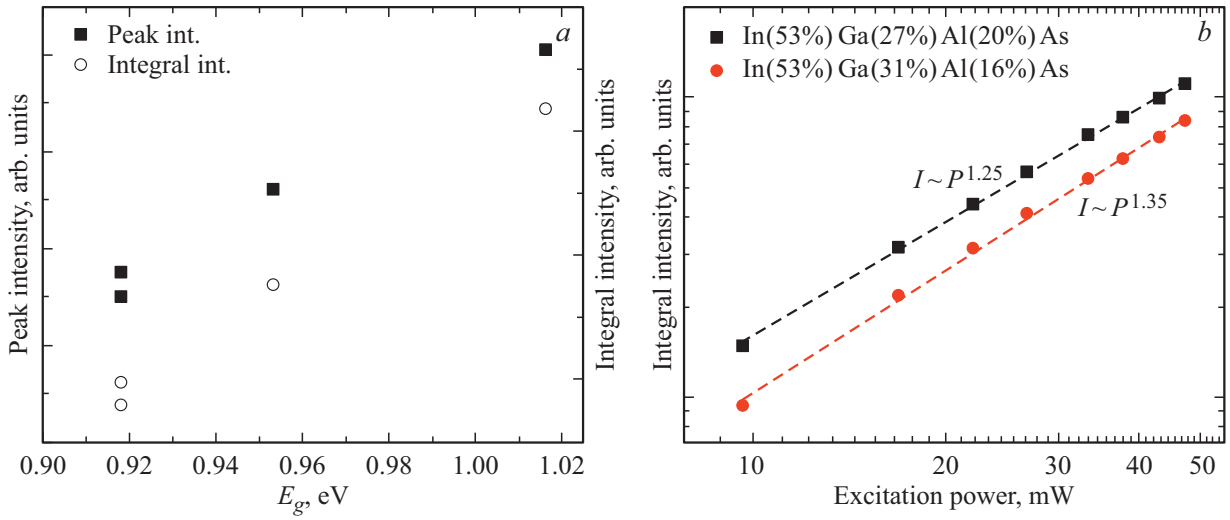

Figure 1. Dependences of the peak/integral intensities on the calculated band gap of the matrix material at an optical pumping level of 46 mW (*a*) and dependence of the integral intensity on the pumping power for heterostructures with matrix/barrier $In_{0.53}Ga_{0.27}Al_{0.20}As$ (1220 nm) and $In_{0.53}Ga_{0.31}Al_{0.16}As$ (1300 nm) layers (*b*).

contribution to the recombination process. The radiative recombination process is dominant at moderate pumping levels. The relative contributions of different recombination processes to emission (1) may be estimated by approximating the dependence of the integral PL intensity on the pumping power with power function P^k. Since the integral PL intensity is proportional to radiative recombination Bn^2, $k \sim 1$ should correspond to the dominance of radiative recombination, while $k \sim 2$ corresponds to the dominance of Shockley–Read–Hall nonradiative recombination.

Figure 1, *b* presents the experimental dependences of the integral PL intensity on optical pumping power P in log-log scale for heterostructures with $In_{0.53}Ga_{0.27}Al_{0.20}As$ (1220 nm) and $In_{0.53}Ga_{0.31}Al_{0.16}As$ (1300 nm) matrices, which exhibited the highest integral PL intensities (Fig. 1, *a*). Index k is close to unity ($k < 1.5$) in both heterostructures; i.e., the PL intensity is almost proportional to the optical pumping power. This is indicative of the fact that nonradiative processes in these heterostructures are much less pronounced than radiative recombination.

At the second stage, the most efficient matrices/barriers were chosen for fabrication of laser heterostructures: $In_{0.53}Ga_{0.27}Al_{0.20}As$ (1220 nm) and $In_{0.53}Ga_{0.31}Al_{0.16}As$ (1300 nm). These layers also served as waveguide ones.

Laser heterostructures were grown by molecular beam epitaxy on an indium phosphide (InP) substrate doped with N^+. Two heterostructures consisting of an emitter $In_{0.52}Al_{0.48}As$ layer with a thickness of 300 nm doped with silicon to a level of $1.0 \cdot 10^{18}$ cm^{-3} and an emitter $In_{0.52}Al_{0.48}As$ layer with a thickness of 700 nm doped with silicon to $5.0 \cdot 10^{17}$ cm^{-3} were grown. This heterostructure design was chosen in order to suppress the probable free-carrier absorption for a light wave penetrating into these layers. An undoped waveguide layer based on InGaAs/InGaAlAs materials with an overall thickness of ~ 630 nm containing an active region based on InGaAs QWs was grown next. A compound *p*-emitter based on $In_{0.52}Al_{0.48}As$ with a thickness of 1500 nm, which consisted of an $In_{0.52}Al_{0.48}As$ layer with a thickness of 1000 nm doped with carbon to a level of $5.0 \cdot 10^{17}$ cm^{-3} and an $In_{0.52}Al_{0.48}As$ layer with a thickness of 500 nm doped with carbon to $1.0 \cdot 10^{18}$ cm^{-3}, was formed after that. A contact $In_{0.53}Ga_{0.47}As$ layer with a thickness of 200 nm doped with carbon to a level of $> 1.0 \cdot 10^{19}$ cm^{-3} provided a quality Ohmic contact. The grown heterostructures differed fundamentally only in the composition of waveguide (matrix/barrier) layers in the active region. Both heterostructures contained seven elastically strained $In_{0.74}Ga_{0.26}As$ QWs, which corresponded to a mismatch parameter (mechanical QW strain) of $\sim 1.4\%$ with the lattice constant of indium phosphide. QWs were separated by barrier InGaAlAs layers with a constant thickness of 12 nm. The composition of InGaAlAs layers in heterostructures differed ($In_{0.53}Ga_{0.27}Al_{0.20}As$ in heterostructure type S1 and $In_{0.53}Ga_{0.31}Al_{0.16}As$ in heterostructure type S2).

Stripe lasers with a stripe contact width of 100 μm were fabricated based on the grown heterostructures in the shallow mesa geometry, where current limiting is established by etching away the top heavily doped $In_{0.53}Ga_{0.47}As$ ~ 200 nm layer. This stripe geometry helped minimize the effect of potential current spread beyond the stripe contact. Individual laser diodes with a cavity length of 0.5, 1.0 and 2.0 mm were fabricated. The cavity was bounded by mirrors formed by cleaving the heterostructure along one crystallographic axis. No additional antireflective and (or) reflective coatings were applied. Laser diodes prepared for measurements were mounted on a copper heat sink (with epitaxial layers facing down) and secured with indium solder. The lasing parameters were examined at different

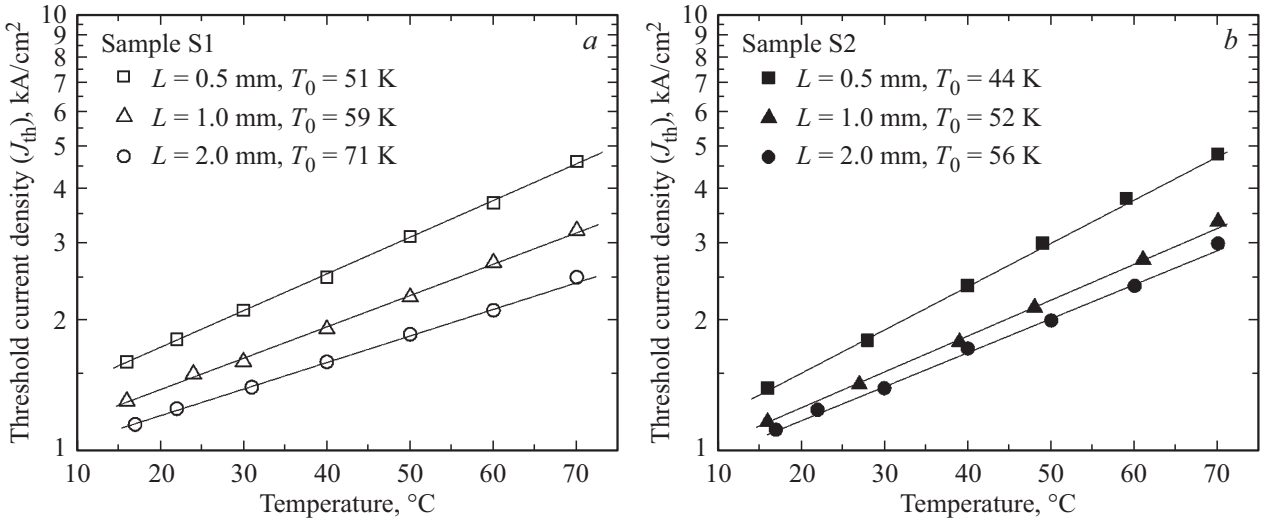

Figure 2. Temperature dependence of the threshold current density for laser diodes with different cavity lengths: *a* — lasers type S1; *b* — lasers type S2.

temperatures and pulsed current pumping with a pulse duration of 0.5−1 μs and a repetition rate of 4−5 kHz.

3. Results and discussion

Figure 2 presents the temperature dependences of the threshold current density for laser diodes type S1 and S2 with different cavity lengths.

The lasing wavelength at 16°C and pumping current $I_{\text{th}} + 0.5$ A was 1559 and 1555 nm for heterostructures S1 and S2, respectively. At a higher temperature of 60°C, the long-wave shift of the wavelength was 28 and 26 nm for heterostructures S1 and S2, respectively. The minimum threshold current density values were measured for samples with a cavity length of 2 mm at a temperature of 17°C: 1.15 kA/cm^2 for lasers type S1 and 1.125 kA/cm^2 for lasers type S2. The temperature stability of a semiconductor laser is traditionally evaluated using characteristic temperature T_0:

$$\frac{1}{T_0} = \frac{1}{J_{\text{th}}} \frac{\partial J_{\text{th}}}{\partial T}, \tag{2}$$

where J_{th} is the threshold current density.

The characteristic temperature estimated in accordance with formula (2) increased from 51 to 71 K (for lasers type S1) and from 44 to 66 K (for lasers type S2) as the cavity length varied from 0.5 to 1.5 mm. Lower values of the characteristic temperature for lasers type S2 are apparently attributable to the weaker localization of carriers in QWs, which, in turn, results from the fact that the band gap of barrier $In_{0.53}Ga_{0.31}Al_{0.16}As$ layers in samples type S2 is narrower than the one in $In_{0.53}Ga_{0.27}Al_{0.20}As$ layers in samples type S1. It is worth noting that the threshold current densities at 17°C for lasers type S2 are lower at all the studied cavity lengths (albeit only slightly). This trend may be shaped by the optical limiting factor in the active region, which is somewhat higher in lasers type S2, since the refraction index of the $In_{0.53}Ga_{0.31}Al_{0.16}As$ layer is higher than the index for $In_{0.53}Ga_{0.27}Al_{0.20}As$. As a result, the waveguide effect in lasers type S2 is stronger. However, this phenomenon warrants further study.

Dynamic parameters of a semiconductor laser depends strongly on the parameters of the gain medium. The resonance laser frequency above the lasing threshold may be calcu;ated using the following formula [18]:

$$f_R = \sqrt{v_g \eta_j g_N / q V_p} \cdot \sqrt{I - I_{\text{th}}}/2\pi, \tag{3}$$

where q is the electron charge, η_j is the current injection efficiency, g_N is the differential gain at the lasing threshold, V_p is the mode volume, and v_g is the group velocity of photons.

It is evident that the attainable resonance frequency increases with g_N:

$$g_N = \frac{\partial G_{\text{th}}}{\partial N} = \frac{\partial G_{\text{th}}}{\partial J_{\text{th}}} \frac{\partial J_{\text{th}}}{\partial N}, \tag{4}$$

where N is the carrier density in cm^{-3} and J_{th} is the threshold current density. In the general case, the threshold current density may be expressed in terms of the carrier density in the active region in the following way [19]:

$$J_{\text{th}} = q N_{qw} (A n_{\text{th}} + B_{2D} n_{\text{th}}^2 + C_{2D} n_{\text{th}}^3), \tag{5}$$

where $n_{\text{th}} = N_{\text{th}} d_a$ is the two-dimensional carrier density in cm^{-2}; N_{qw} is the number of quantum wells in the active region; A is the coefficient of monomolecular recombination via local nonradiative recombination centers (Shockley−Read−Hall nonradiative recombination);

$$B_{2D} = B_{3D} \sqrt{\frac{\frac{m_e + m_h}{2} kT}{\pi \hbar^2}}$$

— is the two-dimensional radiative recombination coefficient expressed in cm$^2 \cdot$ s^{-1}; and C_{2D} is the two-dimensional

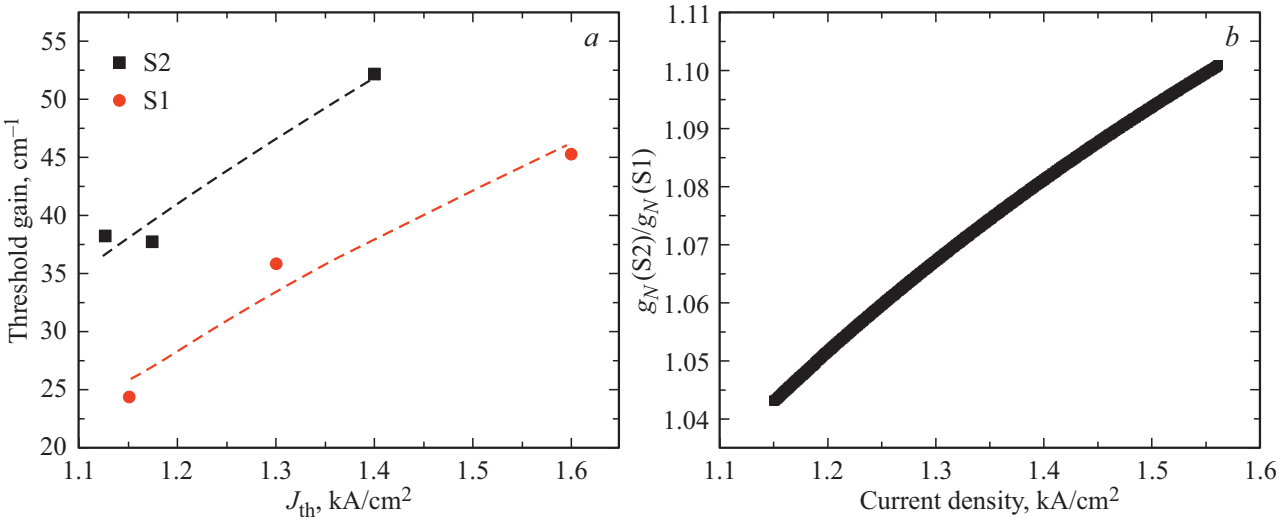

Figure 3. Dependences of the threshold gain on the threshold current of lasers type S1 and S2 and approximation of dependences with formula (8) (*a*) and ratio of the values of differential gain of structures type S1 and S2 (*b*) calculated in accordance with formula (6).

nonradiative Auger recombination coefficient expressed in $cm^4 \cdot s^{-1}$.

At the lasing threshold, monomolecular nonradiative recombination is already significantly weaker than radiative recombination; besides that, radiative recombination is dominant in the emission of test heterostructures that were grown to examine the emission intensity prior to the fabrication of laser heterostructures (see Fig. 1, *b*). In addition, it is known from literature [20] that the primary mechanisms of Auger recombination are suppressed in strained InGaAs/InP QWs with thickness < 3 nm. Thus, we may write

$$J_{\text{th}} = qN_{qw}B_{2D}n_{\text{th}}^2. \tag{6}$$

Taking (4) and (5) into account, we find

$$g_N = \frac{\partial G_{\text{th}}}{\partial N} = \frac{\partial G_{\text{th}}}{\partial J_{\text{th}}} \cdot d_a \frac{\partial J_{\text{th}}}{\partial n_{\text{th}}}$$

$$= \frac{\partial G_{\text{th}}}{\partial J_{\text{th}}} \cdot 2d_a\sqrt{qN_{qw}B_{2D}J_{\text{th}}}. \tag{7}$$

Since radiative recombination coefficient B_{2D} depends only on the material and parameters of QWs [19], it is fair to assume that heterostructures type S1 and S2 have the same value of B_{2D}. The QW thickness is 2.8 nm in structure type S1 and 2.4 nm in structure type S2. Thus, having measured the current dependence of the threshold gain, we may compare the differential gain of samples S1 and S2.

The gain at the lasing threshold is equal to total losses; therefore,

$$\frac{G_{\text{th}}}{\eta_{\text{int}}} = \frac{\alpha_{\text{in}} + \alpha_{\text{out}}}{\eta_{\text{int}}} = \left(\frac{\alpha_{\text{in}} + \alpha_{\text{out}}}{\eta_{\text{int}}\alpha_{\text{out}}}\right)\alpha_{\text{out}} = \frac{\alpha_{\text{out}}}{\eta_{\text{diff}}}, \tag{8}$$

α_{in} — denotes internal radiation losses inside a cavity, $\alpha_{\text{out}} = \frac{1}{2L}\ln\frac{1}{R_1 \cdot R_2}$ — represents radiation output losses, η_{diff} is the differential quantum efficiency, and η_{int} is the internal quantum efficiency of stimulated emission. Thus, having measured η_{diff} and the cavity length for each laser, we may determine the value of G_{th} under the assumption that internal quantum yield G_{th} of stimulated emission is 100%.

The dependences of gain G_{th} at the lasing threshold on the pumping current density, which were determined experimentally and calculated using formulae (2) and (4), are approximated well with the following formula [21]:

$$G_{\text{th}} = G_{0J}\ln(J_{\text{th}}/J_{\text{tr}}), \tag{9}$$

where J_{th} is the threshold current density, J_{tr} is the transparency current density, and G_{0J} is the coefficient of modal optical gain. Figure 3 shows the dependences of threshold gain on the pumping current density of lasers type S1 and S2, the approximation of these dependences with formula (8), and the dependence of ratio $\left(\frac{g_N(S2)}{g_N(S1)}\right)$ of differential gain values of lasers type S1 and S2 (calculated in accordance with formula (7)) on the pumping current density. It can be seen that the obtained ratio is higher than unity; thus, the differential gain of the active medium of lasers type S2 is higher than the one of lasers type S1. In our earlier studies. we have tested VCSELs of the 1550 nm spectral range with an active region based on QWs in an $In_{0.53}Ga_{0.27}Al_{0.20}As$ matrix, which corresponds to the matrix of structures type S1, and found maximum modulation frequencies in excess of 11 GHz [12]. Therefore, the substitution of the $In_{0.53}Ga_{0.27}Al_{0.20}A$ active region matrix in such VCSELs with $In_{0.53}Ga_{0.31}Al_{0.16}As$ should result in additional enhancement of the frequency characteristics of VCSELs of the 1550 nm spectral range.

4. Conclusion

The parameters of optical gain in laser diodes of the 1550 nm spectral range with seven InGaAs quantum wells and different compositions of InGaAlAs waveguide layers were examined. The results of analysis of experimental electroluminescence data revealed that the differential gain of such laser diodes decreases when the molar fraction of aluminum in InGaAlAs layers increases from 0.16 to 0.20 (with the lattice matching of layers with indium phosphide being retained). In our earlier studies. we have tested VCSELs of the 1550 nm spectral range with an active region based on QWs in an $In_{0.53}Ga_{0.27}Al_{0.20}As$ matrix, which corresponds to the matrix/waveguide layers of structures type S1, and found maximum small-signal modulation frequencies in excess of 11 GHz [12]. Therefore, the substitution of the $In_{0.53}Ga_{0.27}Al_{0.20}A$ active region matrix in such VCSELs with $In_{0.53}Ga_{0.31}Al_{0.16}As$ should result in additional enhancement of the frequency characteristics of VCSELs of the 1550 nm spectral range.

Funding

The work of authors from the ITMO University was supported financially by program „Priority 2030“ (with regard to photoluminescence studies) and by the Ministry of Science and Higher Education of the Russian Federation, research project No. 2019.1442 (with regard to the measurement and analysis of steady-state characteristics of laser diodes). A.E. Zhukov and N.V. Kryzhanovskaya acknowledge support from the Fundamental Research Program of the HSE University.

Conflict of interest

The authors declare that they have no conflict of interest.

References

[1] H.R. Ibrahim, M. Ahmed, F. Koyama. *High speed modulation single mode 850 nm DTCC-VCSEL*. In: *24th Microoptics Conf. (MOC)*, Nov. 2019.
[2] N. Ledentsov, Ł. Chorchos, O.Y. Makarov, V.A. Shchukin, V.P. Kalosha, J.-R. Kropp, J.P. Turkiewicz, C. Kottke, V. Jungnickel, R. Freund, N.N. Ledentsov. Electron. Lett., **57** (19), 735 (2021).
[3] D. Bimberg. *Green Nanophotonics for Future Datacom and Ethernet Networks*. In: *Asia Communications and Photonics Conf. 2013* (2013).
[4] S. Spiga, D. Schoke, A. Andrejew, G. Boehm, M.-C. Amann. J. Light. Technol., **35** (15), 3130 (2017).
[5] D. Ellafi, V. Iakovlev, A. Sirbu, G. Suruceanu, Z. Mickovic, A. Caliman, A. Mereuta, E. Kapon. Opt. Express, **22** (26), 32180 (2014).
[6] A.V. Babichev, L.Y. Karachinsky, I.I. Novikov, A.G. Gladyshev, S.A. Blokhin, S. Mikhailov, V. Iakovlev, A. Sirbu, G. Stepniak, L. Chorchos, J.P. Turkiewicz, K.O. Voropaev, A.S. Ionov, M. Agustin, N.N. Ledentsov, A.Y. Egorov. IEEE J. Quant. Electron., **53** (6), 1 (2017).
[7] M. Ortsiefer, W. Hofmann, J. Rosskopf, M.C. Amann. *Long-wavelength VCSELs with buried tunnel junction*. In: *VCSELs* (Springer, Berlin–Heidelberg, 2013) p. 321.
[8] H.-T. Cheng, Y.-C. Yang, T.-H. Liu, C.-H. Wu. Photonics, **9** (2), 107 (2022).
[9] G. Steinle, H. Riechert, A.Y. Egorov. Electron. Lett., **37** (2), 93 (2001).
[10] I.I. Novikov, N.Y. Gordeev, M.V. Maximov, Y.M. Shernyakov, A.E. Zhukov, A.P. Vasil'ev, E.S. Semenova, V.M. Ustinov, N.N. Ledentsov, D. Bimberg, N.D. Zakharov, P. Werner. Semicond. Sci. Technol., **20** (1), 33 (2004).
[11] M. Gębski, D. Dontsova, N. Haghighi, K. Nunna, R. Yanka, A. Johnson, R. Pelzel, J.A. Lott. OSA Contin., **3** (7), 1952 (2020).
[12] S.A. Blokhin, M.A. Bobrov, A.A. Blokhin, A.G. Kuzmenkov, N.A. Maleev, V.M. Ustinov, E.S. Kolodeznyi, S.S. Rochas, A.V. Babichev, I.I. Novikov, A.G. Gladyshev, L.Y. Karachinsky, D.V. Denisov, K.O. Voropaev, A.S. Ionov, A.Y. Egorov. Semiconductors, **53** (8), 1104 (2019).
[13] A. Sirbu, G. Suruceanu, V. Iakovlev, A. Mereuta, Z. Mickovic, A. Caliman, E. Kapon. IEEE Photonics Technol. Lett., **25** (16), 1555 (2013).
[14] E.S. Kolodeznyi, A.S. Kurochkin, S.S. Rochas, A.V. Babichev, I.I. Novikov, A.G. Gladyshev, L.Ya. Karachinsky, A.V. Savelyev, A.Yu. Egorov, D.V. Denisov. Semiconductors, **52** (9), 1156 (2018).
[15] M.V. Maksimov, Yu.M. Shernyakov, F.I. Zubov, I.I. Novikov, A.G. Gladyshev, L.Ya. Karachinsky, D.V. Denisov, S.S. Rochas, E.S. Kolodeznyi, A.Yu. Egorov, A.E. Zhukov. Tech. Phys. Lett., **45** (6), 549 (2019).
[16] S. Karpov. Opt. Quant. Electron., **47** (6), 1293 (2015).
[17] K.R. Poguntke, A.R. Adams. Electron. Lett., **1** (28), 41 (1992).
[18] L.A. Coldren, S.W. Corzine. *Diode lasers and photonic integrated circuits*, ser. Wiley series in microwave and optical engineering (Wiley, N.Y., USA, 1995) p. 73.
[19] L.V. Asryan. Quantum Electron., **35** (12), 1117–1120 (2005).
[20] A.S. Polkovnikov, G.G. Zegrya. PRB, **58** (7), 4039 (1998).
[21] A.E. Zhukov. *Osnovy fiziki i tekhnologii poluprovodnikovykh lazerov* (S.-Peterb., Izd. Akad. Univ., 2016) (in Russian).